

Langmuir probe measurements in an inductively coupled plasma source

A. Schwabedissen, E. C. Benck, and J. R. Roberts

National Institute of Standards and Technology, Gaithersburg, Maryland 20899

(Received 16 September 1996)

Measurements of the plasma potential, electron density, effective electron temperature, and electron energy distribution function (EEDF) have been performed with Langmuir probes in planar, electrostatically shielded, low-pressure inductively coupled plasmas. The plasma source is a modification of the Gaseous Electronics Conference RF Reference Cell [P. J. Hargis *et al.*, Rev. Sci. Instrum. **65**, 140 (1994)] with the upper electrode replaced by a five-turn planar coil and a quartz vacuum interface. Four different rare gases (Ar, Kr, Xe, and Ne), a He:Ar (96:4) mixture, and O₂ and N₂ were investigated. We found that with increasing ionization potential of the rare gas the electron density decreases, while the effective electron temperature and the plasma potential increase. Non-Maxwellian EEDFs were observed for all energies for O₂ and N₂ discharges as well as for the rare gases above the energy range for elastic collisions. Spatially resolved measurements confirm that the EEDF is determined by spatially averaged quantities instead of the local electric field. [S1063-651X(97)09003-X]

PACS number(s): 52.80.Pi, 52.70.Ds, 52.70.Nc

I. INTRODUCTION

Recently there has been considerable research effort in the development of radio-frequency (rf) inductively coupled plasma (ICP) sources, especially for plasma processing applications in the semiconductor industry. There is a need for sources that operate at low pressure (0.1–5 Pa) combined with a high plasma density (10^{11} – 10^{12} cm⁻³) and a high uniformity [1–4]. Low pressure has the advantage that due to fewer collisions in the plasma sheath, the etch anisotropy can be improved, while higher plasma densities lead to faster processing. In capacitively coupled discharges high plasma densities can only be obtained by applying high powers, which are inevitably connected with high sheath voltages and therefore high ion energies, which can cause damage. In contrast to this, the plasma in an ICP can be created with a low sheath voltage. The ion impact energy can be controlled by an external rf bias applied to the wafer electrode [3].

A relatively simple method of ICP excitation consists of using a planar, spiral coil coupling a rf field through a quartz window into the plasma chamber. In the recent past, a large number of basic research papers utilizing this type of ICP have been published. These works include Langmuir probe measurements of ion densities, electron densities and temperatures, electron energy distribution functions (EEDFs) [5–10], dB/dt probe measurements of electric and magnetic fields [11], and emission and laser spectroscopic measurements [12–14]. Argon was used predominantly as the working gas in these experiments and since the work was performed by different groups worldwide, many different reactor geometries and electrical circuits were used.

Experience has demonstrated that experimental data from low-temperature glow discharges have often been difficult to compare when obtained by different research groups using different plasma reactors. To isolate the effects of reactor geometry from other experimental variables, a reference reactor for parallel-plate capacitively coupled rf discharges, the Gaseous Electronics Conference (GEC) RF Reference Cell [15] was developed in the late 1980s and has led to a much

better understanding of the physical and chemical processes in parallel-plate reactors.

Recently Miller *et al.* [16] proposed a design for an inductively coupled plasma source for the GEC RF Reference Cell chamber by replacing the standard upper electrode assembly by a planar coil and a quartz vacuum interface. This design, as in the case of the original GEC reactor, provides satisfactory technical performance and excellent diagnostic access.

The aim of this work is to provide data of important plasma parameters such as the plasma potential, effective electron temperature, electron density, and EEDF for this type of ICP cell for different rare gases as well as nitrogen and oxygen. The measurements were made using cylindrical Langmuir probes. Although argon has the greatest application in plasma processing, the data for the other rare gases are useful for the general understanding of ICPs, which are also used for electrodeless lamps in light source technology. To our knowledge, data for planar coupled ICPs in neon and xenon have not been published so far. In contrast to recent publications where the results are presented as a function of the total incident power [2,4,7,8], all our results are given as a function for the power dissipated in the plasma P_{dis} (also denoted as “plasma power”). We believe that measurements related to P_{dis} provide a better set of defined plasma parameters than those related to the total input power. This is especially true since the measurements may depend to a large extent on the type and characteristics of the induction coil, matching circuit elements, and transmission line.

II. EXPERIMENTAL SETUP

A. Discharge configuration

A detailed sketch of the electrode region of the ICP for the GEC Reference Cell configuration has already been given by Miller *et al.* [16], therefore, we will repeat only the most important dimensions: (i) the distance of the quartz window (thickness 9.5 mm) to the lower electrode is equal to 40.5 mm, (ii) the diameter of the stainless-steel lower elec-

trode plate is equal to 165 mm, (iii) and the inner diameter of the cell chamber is equal to 248 mm. The antenna consists of a five-turn spiral coil (outer diameter 10 cm, inductance 1.3 μH) of 3-mm ($\frac{1}{8}$ -in.) copper tubing that is electrostatically shielded from the plasma by a radially spoked brass foil, similar to the screen described by Mahoney *et al.* [7]. The center of the coil was powered with a frequency of 13.56 MHz and the outside winding was grounded. Between the coil and Faraday shield, a 3-mm-thick ($\frac{1}{8}$ -in.) quartz plate was mounted for electrical insulation. Since the coupling of the coil to the plasma is very sensitive to the positioning and spacing between the coil and coupling window, the coil was pressed against the quartz plate and fixed in place by a slotted five-arm holder that was mounted on the top of the cell. For all measurements the plasma chamber and the stainless-steel lower electrode were grounded. The chamber was pumped with a turbo pump backed by a mechanical pump, giving a base pressure of about 4×10^{-6} Pa. During discharge operation the gas flow was kept constant by using a mass flow controller at 3.7 $\mu\text{mol/s}$ [5.0 sccm (where sccm denotes cubic centimeter per minute at STP)] on the input for all gases, except the heavier rare gases xenon and krypton, which were operated at a flow rate of 1.5 $\mu\text{mol/s}$ (2.0 sccm). In contrast to the capacitively coupled GEC Reference Cell, gas is fed into the plasma chamber not via holes in one electrode but via one of the 7-cm ($2\frac{3}{4}$ -in.) radial flanges.

The coil voltage was measured by a capacitive voltage probe, calibrated (without plasma) with reference to a commercial resistive voltage probe (Phillips PM 8931/09). The coil current was monitored on the grounded lead of the coil by an inductive coupled current probe, also calibrated with reference to a commercial probe (Pearson model 2877). A matching network consisting of two air-dielectric variable capacitors, directly connected to the coil to minimize resistive losses, was utilized [16]. The capacitors were adjusted for minimum reflected power for each plasma condition by means of a rf watt meter. The reflected power P_{refl} was always less than 5% of the input power. As mentioned above, the data are presented as functions of the power dissipated into the plasma P_{dis} , which is the total incident power P_{in} minus reflected power P_{refl} (both determined by the power meter) minus resistive losses $I_{\text{coil}}^2 R_{\text{eff}}$, where R_{eff} is the resistance of the coil and surrounding hardware and I_{coil} the effective rf current ($P_{\text{dis}} = P_{\text{in}} - P_{\text{refl}} - I_{\text{coil}}^2 R_{\text{eff}}$). R_{eff} was determined from the absorbed input power P_{abs} ($P_{\text{abs}} = P_{\text{in}} - P_{\text{refl}} = I_{\text{coil}}^2 R_{\text{eff}}$) with no plasma present. The no-plasma condition was obtained by powering the system under high vacuum. This method slightly overestimates the actual R_{eff} with plasma in the cell since the plasma shields eddy currents induced in the walls and lower electrode. On the other hand, an increase of R_{eff} can be expected with increasing temperature of the coil and the surrounding hardware, so there is some compensation.

As previously described by Miller *et al.* [16], the resistive losses are due in part to currents induced in the stainless-steel cylinder that surrounded the coil (which becomes hot during discharge operation). Therefore, we put a copper sleeve (length 352 mm, height 102 mm, thickness 0.635 mm) between the coil and the surrounding cylinder, which resulted in a reduction of R_{eff} from 1.2 Ω to 0.75 Ω . To prevent overheating of the coil and surrounding hardware, the coil

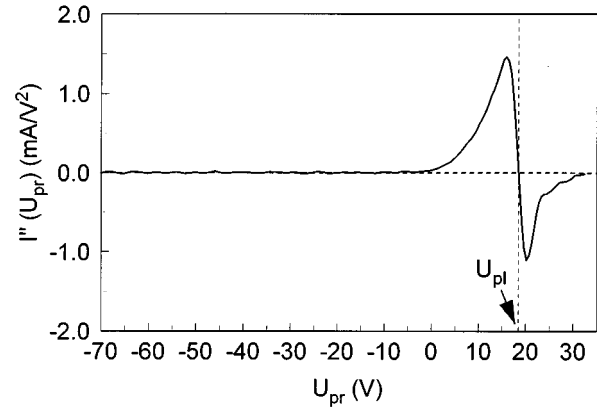


FIG. 1. Second derivative of a current voltage probe characteristic in an argon ICP ($p = 2.66$ Pa, $P_{\text{dis}} = 53$ W).

was internally cooled with chilled water and the whole matchbox-coil unit was cooled by a fan.

B. Langmuir probe setup and data evaluation

It is well known from capacitive rf discharges that a Langmuir probe has to be compensated for the rf fluctuations of the plasma potential to deliver reliable results [17,18]. The plasma potential and also the voltage drop in the probe space-charge sheath are modulated in this type of discharge with amplitudes of typically tens of volts. rf probe currents are usually suppressed by resonant blocking inductors and an additional metallic cylinder, which is connected capacitively to the probe in front of the inductors in order to reduce the capacitive impedance between the probe tip and the plasma [17]. This is also the case for some commercial Langmuir probes, e.g., the one we used (Hiden ESP Mark 2).

The rf plasma potential fluctuations in ICPs are much lower than in capacitive rf discharges. This reduces the efforts necessary for compensation of the probe. With a wire loop probe [19,20] we measured rf (zero-to-peak) amplitudes of less than 1 V at 13.56 MHz for most operating conditions. The amplitudes of the higher harmonics were negligible (less than 0.2 V). The rf amplitudes decreased slightly with input power and increased with lower pressure.

Whether the compensation of the rf voltage drop at the space-charge sheath is sufficient can easily be determined from the second derivative of the probe characteristic [21] $I''(U_{\text{pr}})$, where U_{pr} is the applied voltage to the probe. Ideally, when the probe potential is varied around the plasma potential $I''(U_{\text{pr}})$ should have a single maximum and a single minimum close to each other, i.e., not more than T_e apart. This characteristic was fulfilled for nearly all second derivatives of probe measurements in the inductive discharge mode in the ICP source (see Fig. 1).

The thin wire probe tips (radius 75 μm) were made of tungsten or nickel. The original tip length of 10 mm was shortened to 4.3 mm to prevent the probe tip from glowing red at high plasma densities and high positive probe voltages. The probe support close to the tip is a ceramic tube 1 mm in diameter, which is small compare to the electron mean free path (which is of the order of several centimeters at the investigated pressure range) for all investigated pres-

tures. Therefore, the collisionless-sheath Langmuir probe theory can be applied [22]. A single I - V characteristic with 400 data points was taken in 6 s, averaging over each data point for 15 ms. Between scans the probe was cleaned by plasma ion bombardment by biasing it to -100 V. Using this technique, we obtained reproducible I - V characteristics that did not show time-dependent hysteresis effects. The probe assembly was attached to a manually operated x - y - z manipulator that was mounted to one of the 7-cm ($2\frac{3}{4}$ -in.) side flanges of the cell chamber. The manipulator had a 10.5-cm translation range in the horizontal direction (which is parallel to the surface of the quartz vacuum interface) and a 2.54-cm (1-in.) range in the vertical direction, perpendicular to the probe axis.

Since the (electron) current of I - V scans in ICPs can be several tens of milliamps or larger, the dc series resistance R of the probe system has to be taken into account. The voltage at the probe tip U_{pr} is determined by

$$U_{\text{pr}} = V - RI(V), \quad (1)$$

where V and I are the output voltage and current of the acquisition electronics, respectively. We determined R to be 10 Ω . U_{pr} is then determined by Eq. (1).

To analyze the probe data, a program called PPA, written by Petig [23], was used. This program has algorithms for smoothing the original data by digital filtering and calculating first and second derivatives $I'(U_{\text{pr}})$ and $I''(U_{\text{pr}})$. After substitution of U_{pr} for V , the voltage increment was no longer a constant. Since PPA requires constant increments, new voltage points were recalculated by means of numerical interpolation. The plasma potential U_{pl} was calculated from the zero crossing of the second derivative of the current-voltage characteristic $I(U_{\text{pr}})$ (see Fig. 1). In most cases this value was identical to the mean value of the voltages of the first maximum and minimum. Druyvesteyn has shown a relation between the EEDF $F(U)$ and the second derivative of the current voltage characteristic [24]

$$F(U) = \frac{\sqrt{-U}(d^2I/dU^2)}{\int_{-\infty}^0 \sqrt{-U}(d^2I/dU^2)dU}, \quad (2)$$

where $U = U_{\text{pr}} - U_{\text{pl}}$. The effective electron temperature T_{eff} (corresponding to a mean electron energy $\langle \epsilon \rangle$) has been calculated by integrating over the EEDF according to

$$\begin{aligned} T_{\text{eff}} &= \frac{2}{3} \langle \epsilon \rangle = \frac{2}{3} e \int_{-\infty}^0 U F(U) dU \\ &= \frac{\frac{2}{3} e \int_{-\infty}^0 (-U)^{3/2} (d^2I/dU^2) dU}{\int_{-\infty}^0 (-U)^{1/2} (d^2I/dU^2) dU}. \end{aligned} \quad (3)$$

The electron density N_e is likewise calculated from the second derivative by

$$N_e = \sqrt{\frac{8m_e}{e^3}} \frac{1}{A_{\text{pr}}} \int_{-\infty}^0 \sqrt{-U} \frac{d^2I}{dU^2} dU, \quad (4)$$

where e and m_e are the charge and mass of an electron and A_{pr} is the probe surface area. Because in low-pressure glow discharges the EEDF is generally non-Maxwellian, the ‘‘Druyvesteyn procedure’’ [Eqs. (2)–(4)] is a more reliable method for probe data analysis than the classical Langmuir procedure [25]. The positive-ion density N_{ion}^+ was calculated from the ion saturation current $I_{\text{ion}}^+(U)$ by fitting a power law to the probe current

$$I_{\text{ion}}^+(U) = N_{\text{ion}}^+ A_{\text{pr}} \sqrt{\frac{e^3 \check{T}_e}{m_{\text{ion}}}} \left(1 - \frac{U}{\check{T}_e}\right)^\gamma, \quad (5)$$

where m_{ion} is the ion mass and \check{T}_e the so-called screening temperature [25,26]. In the orbital-motion-limited theory [22] the exponent γ has a fixed value of 0.5, but PPA can also calculate a least-squares fit for a variable γ to the measured data (modified orbital motion limited theory).

The method of the second derivative can lead to incorrect results when there are negative ions in the plasma, e.g., as in oxygen discharges. For an estimate of the contribution of the negative ions to the total current, we use the classical Langmuir procedure [22], which calculates the electron density from the current I_e at the plasma potential

$$I_e(U_{\text{pl}}) = eN_e A_{\text{pr}} \sqrt{\frac{T_e}{2\pi m_e}}. \quad (6)$$

It should be mentioned that Eq. (6) assumes a Maxwellian EEDF with T_e as the electron temperature. A similar formula can be obtained for the current of the negative ions I_{ion}^- . The ratio between the negative-ion current and the electron current at the plasma potential is then given by

$$\frac{I_{\text{ion}}^-}{I_e} = \frac{N_{\text{ion}}^-}{N_e} \left(\frac{T_{\text{ion}}^- m_e}{T_e m_{\text{ion}}}\right)^{1/2}, \quad (7)$$

where N_{ion}^- and T_{ion}^- are the density and temperature of the negative ions, respectively. Implications of Eq. (7) will be discussed in Sec. III B.

The combination of probe hardware and data analysis software (with digital filtering) resulted in calculated EEDFs with a dynamic range of two to three orders of magnitude. We found the following standard uncertainties σ (given by statistical errors) of the plasma parameters when running the discharge at different times under the same conditions (total input power, pressure, and gas flow rate): plasma potential, relative standard uncertainty less than 4%; effective electron temperature, relative standard uncertainty less than 5%; and electron density, relative standard uncertainty less than 14%. Taking into account the uncertainty of the probe surface area (with a systematic error of 6%) the total relative standard uncertainty of the electron density amounts to 20%.

III. EXPERIMENTAL RESULTS

A. Electrical characteristics of the discharge

Initial experiments were performed with no electrostatic shield between the coil and the plasma. Similar to Miller’s observations, we also found a visible coating of the lower electrode after running the discharge for several hours in the

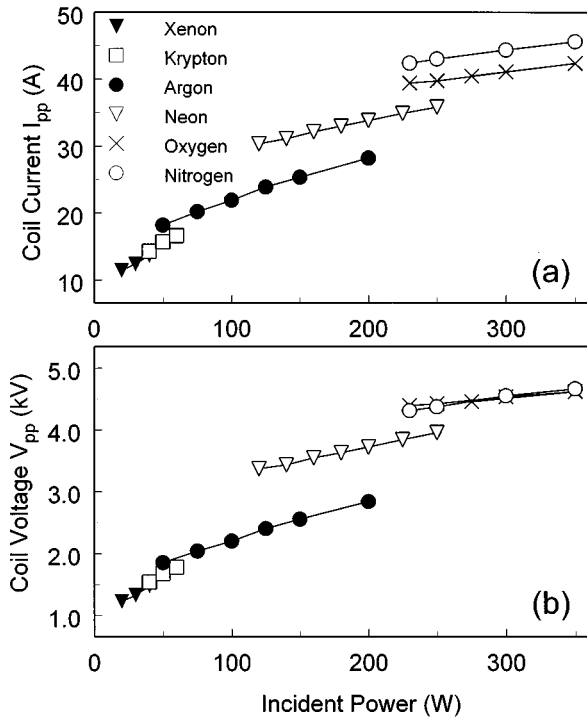


FIG. 2. Peak-to-peak coil voltage and current in the inductive mode for various gases at $p=2.66$ Pa.

inductive mode [16]. Emission spectra of pure argon discharges also showed Si, O, Fe, and Ni atomic transitions. We assume that these impurities are due to sputtering near the upper quartz vacuum interface and the lower stainless-steel electrode. To reduce the sputtering we installed the electrostatic shield. However, with the shield installed, the discharge would no longer self-ignite in the dim, capacitive mode. Therefore, a Tesla coil was used to start the inductive discharges. The total incident power P_{in} needed to ignite and maintain an inductive discharge varied strongly with the gas type: xenon ignited at approximately 30 W, argon at 60 W, neon at 130 W, and nitrogen ignited at 320 W. After ignition, the coil power could be reduced about 10–20 %, while the discharge was still running in the inductive mode. Although the coil was electrostatically screened, weak capacitive discharges were observed when the coil power was reduced below the threshold for inductive discharges, for example, in nitrogen at powers below 230 W. We were not able to start a discharge in pure oxygen. Therefore, we started with an $O_2:Ar$ (1:1) mixture to initiate the discharge, afterward slowly reducing the partial pressure of argon to zero. It was not possible to run pure helium or hydrogen discharges by using the same method; even at very high coil voltages (peak-to-peak voltages $V_{pp} \sim 5$ kV) and input power ($P_{in} > 350$ W), the discharge extinguished after switching off the argon gas flow. After installing the electrostatic screen, the rate of sputtering in pure rare gases was noticeably reduced; however, after running discharges in oxygen and nitrogen at high coil voltages for several tens of hours, deposition was found again on the lower electrode, the quartz vacuum interface, and the walls.

The rf voltages and currents (peak-to-peak values) in the inductive discharge mode for the different rare gases inves-

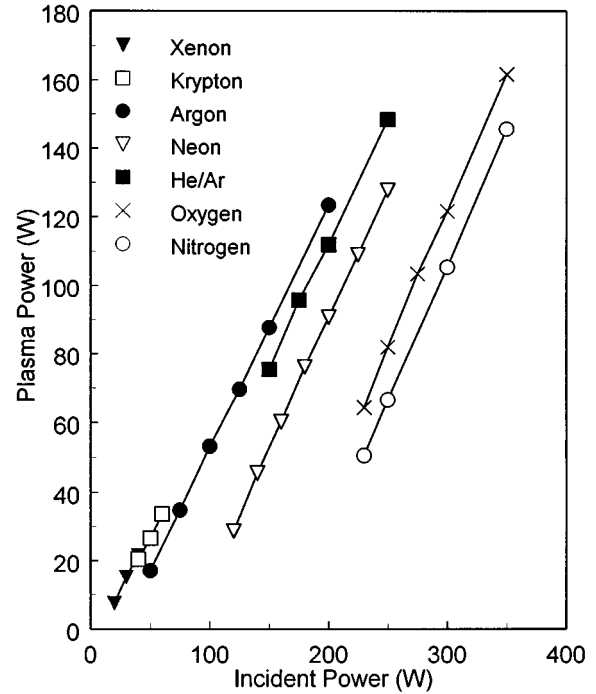


FIG. 3. Power deposited into the plasma in the inductive mode as a function of the total incident power for the different gases at $p=2.66$ Pa.

tigated increased with increasing ionization potential E_i ; xenon ($E_i = 12.1$ eV) has the lowest voltage and current values, followed by krypton ($E_i = 14.0$ eV) and argon (15.8 eV) [see Figs. 2(a) and 2(b)]. Consistent with the jump in the ionization potential, the coil voltages for neon ($E_i = 21.6$ eV) discharges are significantly higher than the heavier rare gases. Both the coil voltage and current increase with decreasing gas pressure for all rare gases. The plasma power coupling efficiency η ($= P_{dis}/P_{in}$) is nearly 65% for the heavier rare gases, but drops down to 30% near the threshold for the inductive mode operation (see Figs. 3 and 4).

To prevent arcing through the quartz plate and due to the large amount of heat developed inside the stainless-steel cylinder surrounding the coil, we did not investigate discharges with total incident powers P_{in} of more than 350 W. The upper power limit in rare-gas discharges (with higher electron densities) was due to the maximum Langmuir probe current (~ 70 mA). Above this current the probe tip glowed red or melted. Also, care had to be taken that the plasma electrons were not depleted in the vicinity of the probe at high probe currents.

B. Plasma parameters on the discharge axis

Figure 5 shows the electron density on the discharge axis (12 mm above the lower electrode and 41 mm below the induction coil), as determined from Eq. (7), for different gases at 2.66 Pa. As can be seen from Fig. 6, the electron densities increase nearly linearly with plasma power P_{dis} as well as increasing with pressure. This behavior was observed for all rare gases. The maximum electron density that can be measured without destroying (melting) the probe tip is about $6 \times 10^{11} \text{ cm}^{-3}$.

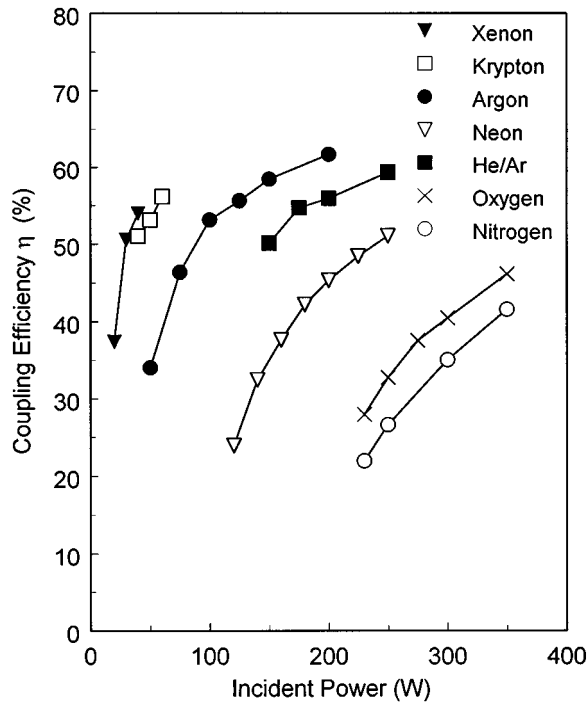


FIG. 4. Coupling efficiency in the inductive mode as a function of the total incident power for the different gases at $p = 2.66$ Pa.

We also observed that oxygen and nitrogen show a linear increase of electron density with plasma power, but no clear dependence on pressure. The electron densities in oxygen and nitrogen discharges are at least one order of magnitude lower than pure argon discharges. O_2 , in contrast to SF_6 and Cl_2 is classified as a weak electronegative gas. The mean electron energies in oxygen discharges are in an appropriate range (between 4 and 9 eV, depending on gas pressure) to produce negative ions by dissociative attachment that has a peak in the cross section at about 6.5 eV [27]. However, the binding energy of the additional electron is only 1.4 eV and new measurements of the electron-impact detachment ($e + O^- \Rightarrow O + 2e$) cross section [28] indicate that the detachment rate for this reaction will be of the same order of magnitude. An additional destruction channel for O^- is the detachment reaction with neutral atoms ($O^- + O \Rightarrow O_2 + e$) that has a large rate coefficient [29]. Therefore, O^- is rapidly depleted from the plasma by these processes. Even under the assumption that the O^- density is equal to the electron density N_e , one obtains from Eq. (7) that the negative-ion current is less than 1% of the electron current at the plasma potential, using an estimated value of 0.1 eV for T_{ion}^- , in correspondence with the experimental results for Ar^+ ions in planar ICPs [13,30]. Furthermore, we did not observe a sharp peak of the second derivative just below the plasma potential, a feature that has been reported for probe measurements of dc glow discharges in oxygen (at higher pressures and lower electron densities) and in $Ar:I_2$ mixtures as a manifestation of large negative-ion concentrations [31,32]. Therefore, we assume that a correction of the measured electron density due to negative ions is not necessary.

Figure 7 shows the behavior of the plasma potential and the effective electron temperature at different plasma powers

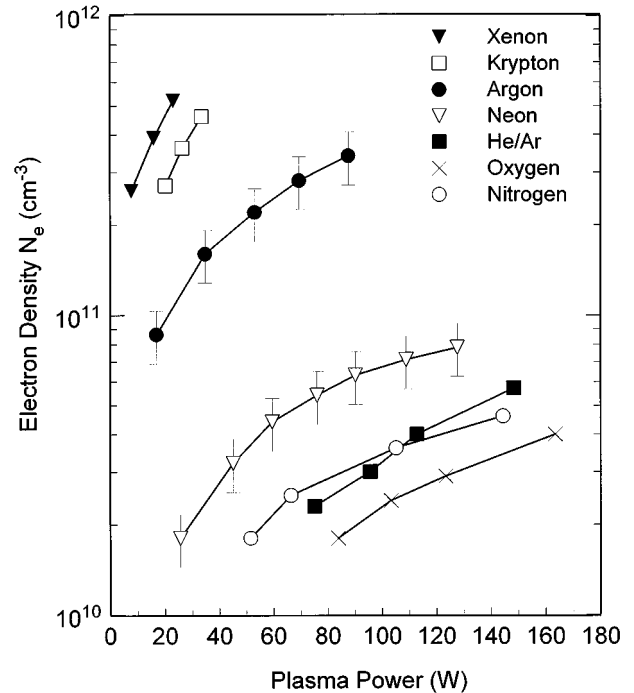


FIG. 5. Electron densities on the discharge axis as a function of the plasma power for different gases at $p = 2.66$ Pa. The error bars for neon and argon are representative for the uncertainty in the electron density measurements.

for neon. The trends are the same as those reported in previous studies of argon ICPs [6,16]. For all gases both of these plasma parameters are fairly independent of power, but they decrease with increasing pressure (see Fig. 8). Again, the

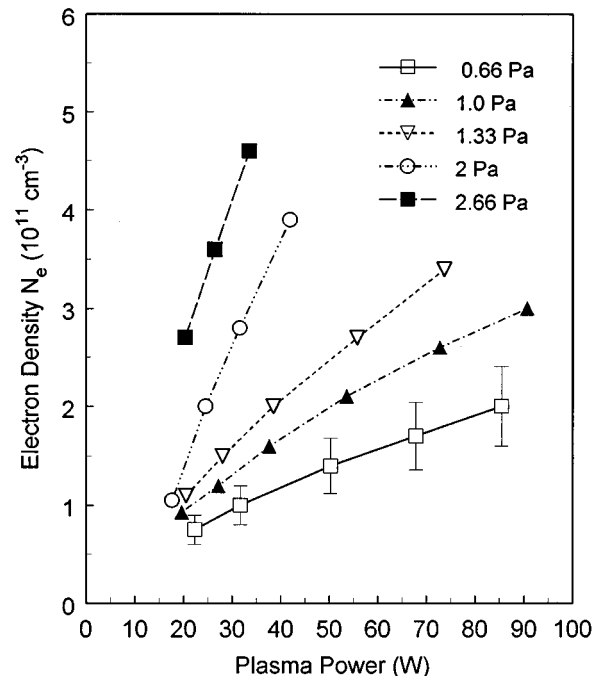


FIG. 6. Electron densities of krypton discharges on the discharge axis as a function of the plasma power for various pressures.

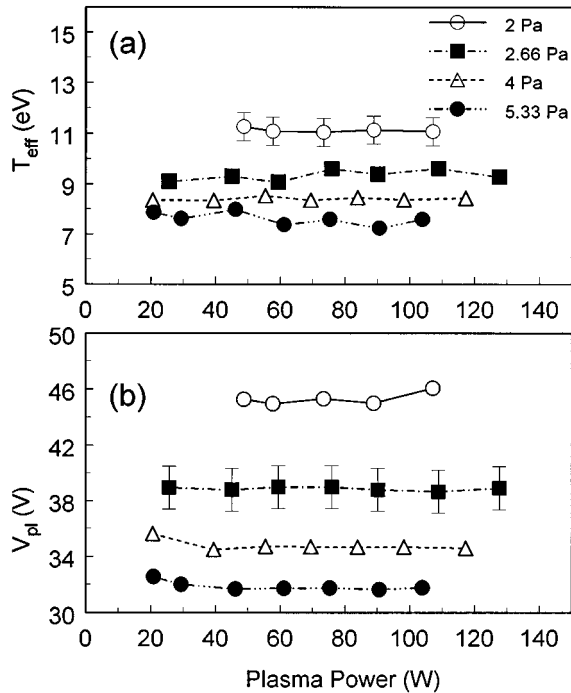


FIG. 7. (a) Effective electron temperature and (b) plasma potential of neon discharges on the discharge axis as functions of the plasma power for different pressures.

values for different rare gases are consistent; the lower the ionization potential of the gas, the lower the effective electron temperature and the plasma potential at a fixed pressure. The effective electron temperature spans a range from 1.8 eV (xenon at 2.66 Pa) up to 11 eV (neon at 2.0 Pa) and the plasma potential from 8 V up to 45 V. Neon shows a rather drastic increase in both parameters compared to the heavier rare gases xenon and krypton. The He:Ar mixtures has lower effective electron temperatures than neon, indicating that the ionization kinetics are dominated by direct or stepwise argon ionization. Because the ionization potential E_i of helium is larger than the E_i of the other rare gases, we expect a pure helium discharge to have much higher electron energies than the 96%:4% He:Ar mixture and those of neon. The increase of the effective electron temperature with decreasing pressure is caused by the lower rate of inelastic electron-heavy particle collisions. This in turn influences the plasma potential because the rate of high-energy electrons escaping to the wall increases, a loss of negative charge that leads to an increase of the plasma potential. The plasma potential is always positive since both ions and electrons tend to diffuse out of the plasma, but the electrons have much higher mobility, so a slight positive space charge develops in the volume.

When reducing the argon gas flow from 3.7 $\mu\text{mol/s}$ (5 sccm) down to 0.75 $\mu\text{mol/s}$ a nearly linear increase of the electron density in the center of the discharge of about 20% was observed, while the plasma potential decreases by about 9%. The effective electron temperature remained unchanged.

C. Radially and axially resolved measurements

Figures 9(a)–9(d) show the radial distribution of several plasma parameters in a krypton discharge. Due to the restric-

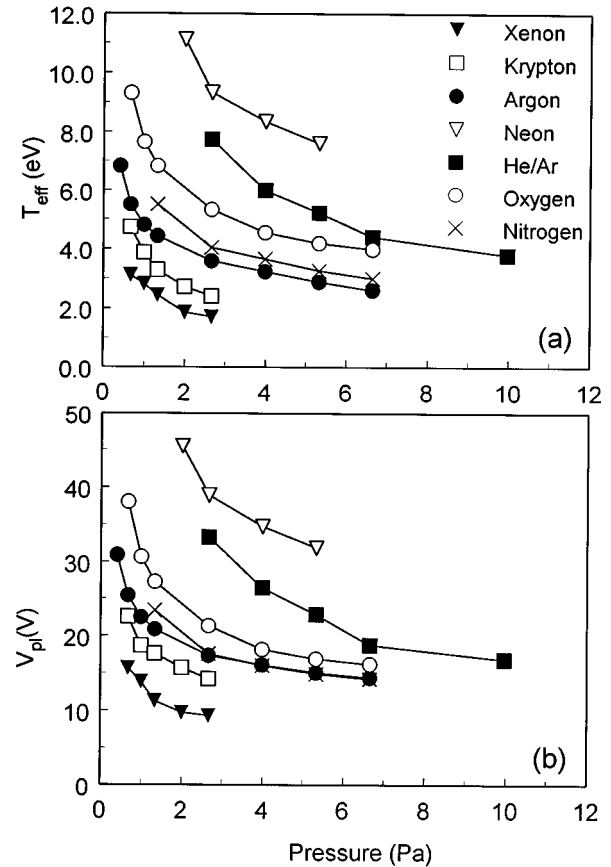


FIG. 8. Average values of (a) the effective electron temperature and (b) the plasma potential on the discharge axis as functions of the gas pressure for different gases.

tion in the travel length of the probe manipulator, it was not possible to perform a scan over the whole diameter of the lower electrode. The electron density is nonuniform over the diameter that is typical for an ambipolar diffusion dominated plasma. The induced electric field in a planar coupled ICP is directed primarily in the azimuthal direction [6]. Due to the curvature of this field, the electrons experience a centrifugal force. This force is balanced by a centripetal force, which is due to the static electric field, resulting from the space charge that develops when the electrons are moving outward. The radial plasma potential distribution [see Fig. 9(d)] forms a potential well that traps most of the electrons. The resulting shape of the radial electron density distribution [Fig. 9(a)] is similar to the shape of the radial plasma potential distribution [Fig. 9(d)].

The plasma potential distribution shown in Fig. 9(d) results in an average radial electric-field strength of 1.1 V/cm. We observed that this radial field strength increases with decreasing pressure. O'Neill, Barnes, and Keller [13] found that the ion translational temperature can be explained by the energy ions gain in this static radial electric field.

The effective electron temperature is constant within the radius of the induction coil (~ 5 cm) and then decreases towards the wall, i.e., it does not follow the local field distribution. The reason for this behavior has already been pointed out by Kortshagen, Pukropski, and Zethoff [8]. The EEDF (and therefore also the effective electron temperature) is determined only by spatially averaged quantities, in particular

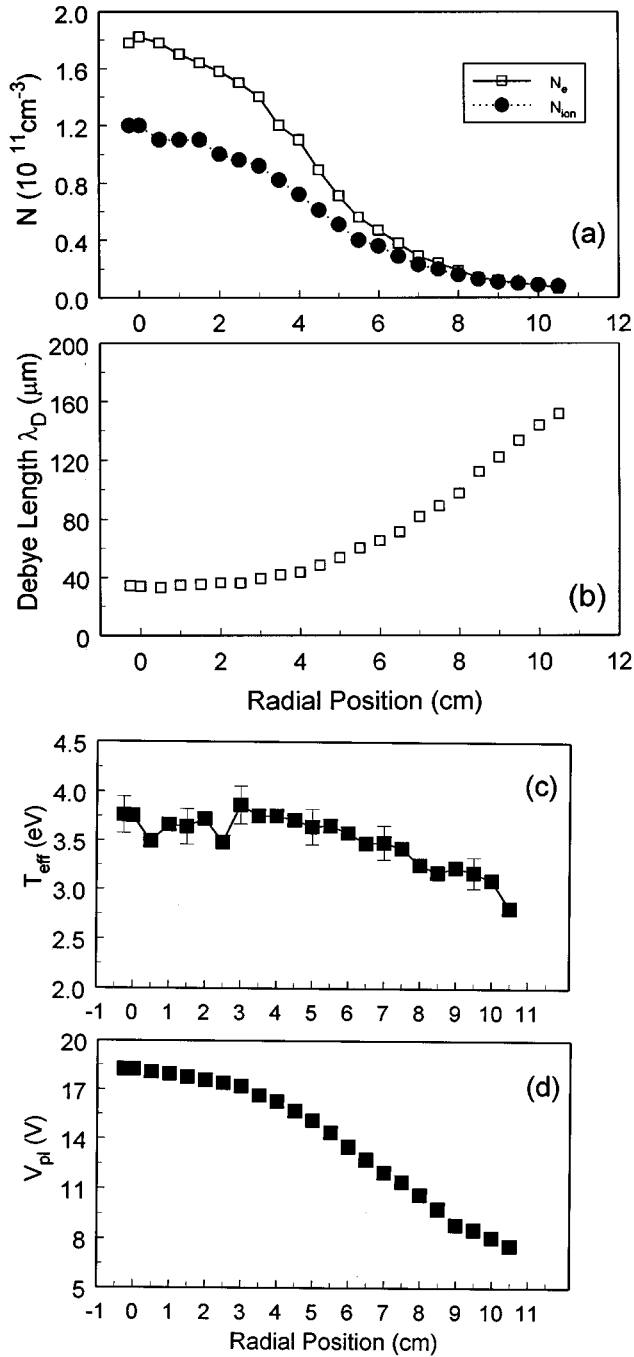


FIG. 9. (a) Electron and ion densities, (b) Debye lengths, (c) effective electron temperature, and (d) plasma potential as functions of the distance from the discharge axis in a krypton discharge at $p=1.33$ Pa and $P_{dis}=32$ W.

by a spatially averaged field, because of the large mean free path λ_{MFP} of the electrons at these relatively low pressures. As there are no nearby confining walls in the chamber, we assume, in agreement with Miller *et al.* [16], that the decrease of electron temperature at radii greater than the coil radius is caused by volumetric expansion.

In a pure rare-gas low-pressure discharge, the relation between the electron (N_e) and positive-ion density (N_{ion}^+) should be near unity in the bulk plasma. As can be seen from Fig. 9(a), the measured positive-ion density is smaller than

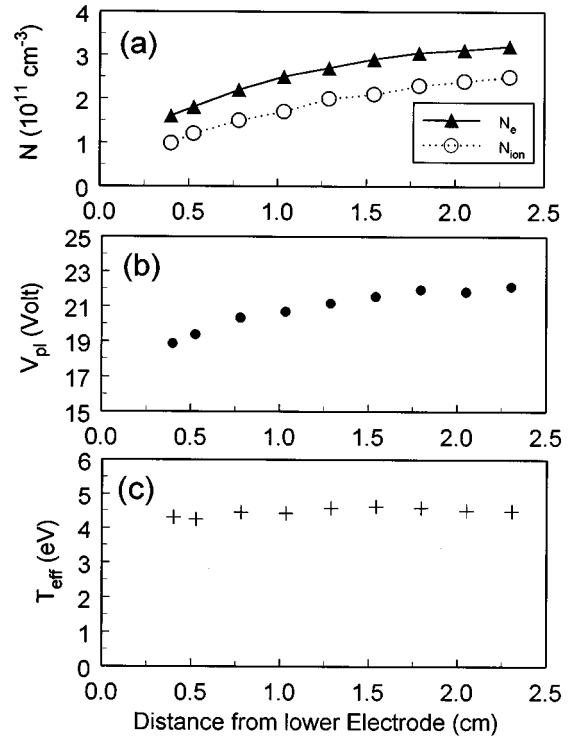


FIG. 10. (a) Electron density, (b) plasma potential, and (c) effective electron temperature on the discharge axis as functions of the distance from the lower electrode in an argon plasma at $p=1.33$ Pa and $P_{dis}=84$ W.

the measured electron density near the center of the discharge if the orbital-motion-limited (OML) theory is used to calculate the ion density. As already discussed by Godyak, Piejak, and Alexandrovich [18] and other authors, the OML theory has many assumptions that are difficult to satisfy under actual experimental conditions. One of these assumptions that can be easily verified is that the Debye length λ_D should be large compared to the probe radius ($75 \mu\text{m}$). Due to the higher electron density, this inequality is not fulfilled in the center of the discharge at the given plasma conditions. At larger radii the Debye length [see Fig. 9(b)] increases and therefore quasineutrality is almost fulfilled. At larger radii N_{ion} is 30–60% higher than N_e , a value that seems to be reasonable taking into account that N_{ion} will be too large due to secondary electrons released by photons, metastable atoms, and ions on the probe surface, while N_e will be too small due to electron reflection and reemission from the probe.

The shape of the radial distribution varies only slightly with pressure or gas type, that is, within the investigated pressure range from 0.66 to 2.64 Pa (5–20 torr). For example, in argon, the half-width at half maximum of the electron density increases from 3.9 cm at 2.66 Pa to 5 cm at 0.66 Pa.

Figure 10 shows an axial scan, limited by the vertical travel capacity of the manipulator (2.5 cm). In the axial direction, the effective electron temperature is likewise nearly constant, while the electron density and plasma potential increase towards the coil.

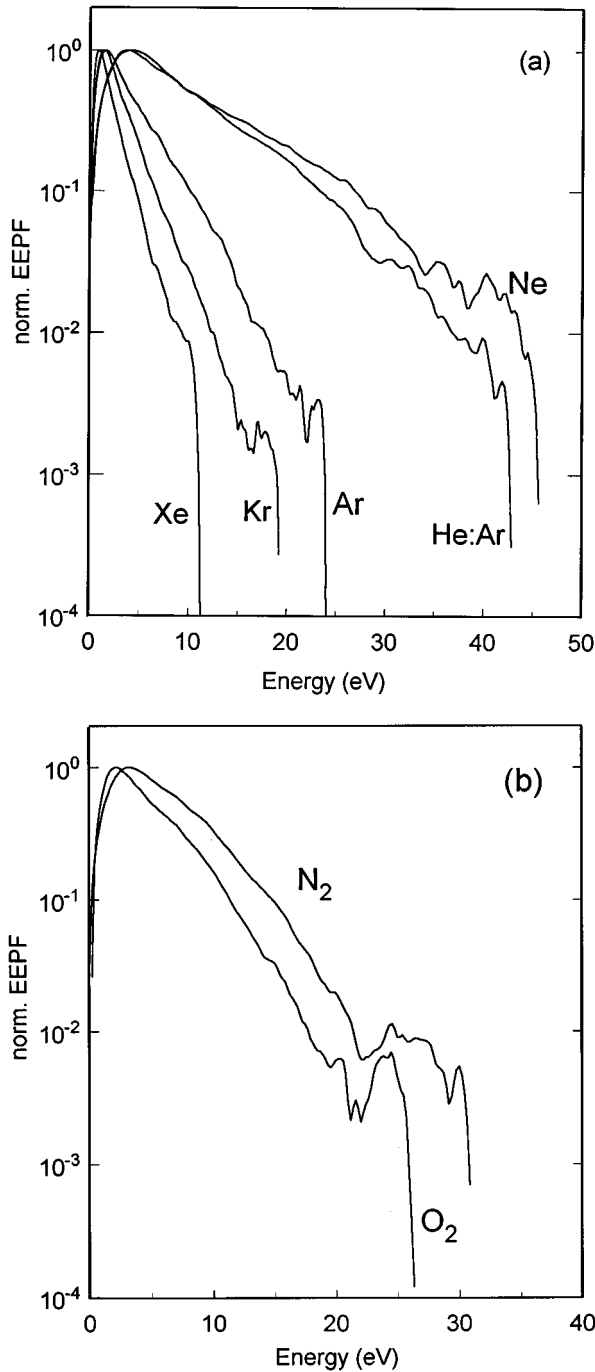


FIG. 11. Electron energy probability functions, normalized to their maximum value for (a) the rare gases and (b) oxygen and nitrogen at $p = 2.66$ Pa.

D. Electron energy distribution and probability functions

The electron energy probability functions (EPPFs), designated by $f(U)$, in the center region of the discharge are presented in Fig. 11. The EEDF, designated by $F(U)$, is related to the EPPF by

$$f(U) = F(U)(-U)^{-1/2}. \quad (8)$$

The advantage of the EPPF plot is that on a semilogarithmic scale, a Maxwellian distribution results in a straight line. The EPPFs for the rare gases and the He:Ar mixture exhibit Max-

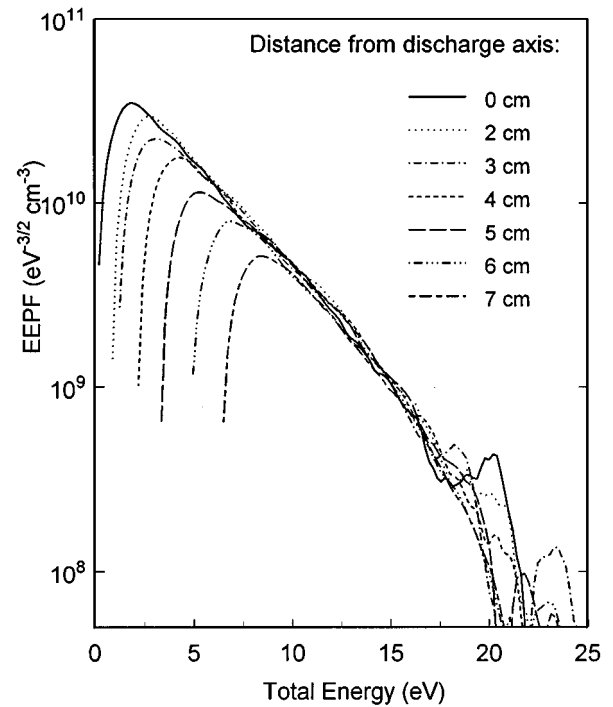


FIG. 12. Electron energy probability functions as a function of the total energy for different distances from the discharge axis in a krypton discharge at $p = 1.33$ Pa and $P_{\text{dis}} = 42$ W.

wellian distributions in the elastic energy range only, that is, the energy range within which inelastic electron atom collisions, such as excitation and ionization, are absent. At higher electron energies, the EPPFs are underpopulated compared to a Maxwellian distribution due to excitation and ionization processes, but also due to the escape of high-energy electrons to the wall. This depletion occurs for each rare gas somewhere between the excitation threshold and the ionization energy. Similar results have been reported by Godyak, Piejak, and Alexandrovich [33] in argon inductive discharges. Model calculations [34] have shown that the relatively large degree of ionization in ICPs (10^{-4} and greater) and therefore the large energy transfer in Coulomb collisions result in the Maxwellian EEDF in the elastic energy range. We believe that the structures in the high-energy part of the EPPFs are caused by noise and the influence of the (positive-) ion current. The EEDFs in nitrogen and oxygen discharges are non-Maxwellian for the entire energy range [see Fig. 11(b)]. When fitting the general distribution

$$F(U) \sim a \exp\left[-\left(\frac{eU}{E_0}\right)^\xi\right] \quad (9)$$

to the second derivatives, where a , E_0 , and ξ are fit factors (a Maxwellian is a special case of this distribution with $\xi = 1$ and $E_0 = kT_e$), exponential factors ξ between 1.2 and 1.6 are obtained for oxygen, with a trend towards a Maxwellian distribution for lower pressures. Nitrogen, on the other hand, shows the reverse trend; the exponents increase with decreasing pressure to values of 1.4 at $p = 1.33$ Pa and are nearly Maxwellian at $p = 5$ Pa.

Figure 12 shows a group of graphs of the measured EE-

TABLE I. Comparison of plasma parameters measured by different groups in ICPs.

Reference	Argon				Oxygen			
	0.66 Pa	1.33 Pa		2.66 Pa		0.66 Pa	1.33 Pa	
	T_e (eV)	T_e (eV)	V_{pl} (V)	N_e (cm ⁻³)	T_e (eV)	V_{pl} (V)	T_e (eV)	T_e (eV)
[4]							7.7	6.8
[33]	6.0	4.9			4.0			
[7]		4.7	17.9		3.9	16.7		
[14]	2.8	2.4			2.0			
[6]	4.9	4.0			3.0			
[16]		4.2	20.1	4.0×10^{11}				
This work	5.5	4.4	20.9	2.6×10^{11}	3.6	17.3	9.3	6.8

PFs as a function of the total energy of the electrons for different radial positions within the plasma. Because the plasma potential is decreasing towards the wall, the potential energy of electrons compared to the discharge center (equal to the zero of the potential energy) is increasing when moving outward. In Fig. 12 the zeros of the kinetic energies of the EEPFs are shifted according to the measured shift of the plasma potential relative to the center, i.e., according to the value of the potential energy the electrons gain when they move outward. Since the high-energy parts of all EEPFs correspond with each other within the experimental error, this is a confirmation of the validity of the nonlocal field approach [8,35]. The nonlocal field approach specifies that for the formation of the EEDF for pressures typical of ICPs (5 Pa and below) only the spatially averaged rf electric field is responsible rather than the local electric-field strength. For example, on the discharge axis, the magnitude of the induced electric field is very small [11]. Nevertheless, the mean electron energy is typically several eV due to nonlocal heating effects.

E. Comparison with other results

Table I compares the results from other groups using planar ICPs with this work. As the effective electron temperature and the plasma potential are essentially a function of the total gas pressure only, these parameters should be comparable. The electron densities, however, depend on the individual reactor geometry and power dissipated into the plasma, hence only a comparison with the results of Miller *et al.* [16] can be made. While the plasma potential and electron temperature are in good agreement, our measured electron densities are 35% lower than the densities of Miller *et al.* at the same plasma power and pressure. A possible reason for the lower electron density could be the electrostatic shield used in our setup, which increases the distance between the coil and the plasma, hence reducing the coupling efficiency. On the other hand, there is good agreement in the electron temperatures that were obtained from Langmuir probes. The electron temperatures measured by Hori *et al.* [14] from Thompson scattering are lower than all measurements done with Langmuir probes. A possible explanation for this discrepancy could be the non-Maxwellian char-

acter of the EEDF above the energy range for elastic collisions. In this high-energy region the slope of the EEPF is steeper than at low energies [see Fig. 11(a) and Ref. [33]], which is equivalent to a lower temperature of the high-energy electrons. Thompson scattering, however, is more sensitive to the high-energy electrons. Hori *et al.* [14] have calculated their electron temperatures from a semilogarithmic plot of the detected signal vs $(\Delta\lambda)^2$, where $\Delta\lambda$ is the difference in wavelengths between the laser wavelength (532 nm) and the scattered wavelength. Most of their data points are in the interval $(\Delta\lambda)^2 = 5-25 \text{ nm}^2$, which corresponds to electron energies between 8 and 35 eV. Thus these measurements correspond to the higher-energy region of the EEDF.

IV. CONCLUSION

In this paper an ICP using a GEC RF Reference Cell chamber has been characterized for a broad range of discharge parameters with a Langmuir probe. The plasma parameters in an ICP using several different gases were investigated and compared. In order to provide a better set of defined plasma parameters, we present our results as a function of the power dissipated into the plasma P_{dis} . Our results may therefore be useful as reference data for other planar ICPs, especially for planar ICPs using the GEC RF Reference Cell chamber.

We observed that the input power needed to maintain an inductive discharge varies drastically with the working gas. The measured electron densities of the molecular gases O_2 and N_2 were at least one order of magnitude below those of argon. On the other hand, the electron densities of krypton and xenon discharges are significantly higher than argon discharges at the same plasma power. So it may be advantageous to replace argon by krypton or xenon in certain plasma processing applications. Helium and neon, however, are not well suited to generate the desirable plasma densities in the range of $10^{11}-10^{12} \text{ cm}^{-3}$.

The underpopulation of the high-energy tail of the EEDF we found for all rare gases and the non-Maxwellian EEDFs of nitrogen and oxygen for the entire energy range are important for model calculations. An extrapolation of the EEDF from the elastic energy range into the inelastic energy range

may cause a significant error in the calculation of excitation and ionization rates in these non-Maxwellian plasmas.

ACKNOWLEDGMENTS

We thank Dr. M. Sobolewski (NIST) for lending us the Hidden Langmuir probe and for measuring the coil resistance and inductance and the rf plasma potential. We are grateful to Professor K. Wiesemann (Ruhr-Universität, Bochum, Germany) for providing the Langmuir probe data analysis pro-

gram PPA. A.S. thanks the Alexander von Humboldt Foundation for financial support.

Certain commercial equipment, instruments, or materials are identified in this paper to specify adequately the experimental procedure. Such identification does not imply recommendation or endorsement by the National Institute of Standards and Technology, nor does it imply that the materials or equipment identified are necessarily the best available for the purpose.

-
- [1] J. S. Ogle, U.S. Patent No. 4,948,458 (14 August 1990).
- [2] J. Hopwood, *Plasma Sources Sci. Technol.* **1**, 109 (1992).
- [3] J. H. Keller, J. C. Forster, and M. S. Barnes, *J. Vac. Sci. Technol. A* **11**, 2487 (1993).
- [4] M. S. Barnes, J. C. Forster, and J. H. Keller, *Appl. Phys. Lett.* **62**, 2622 (1993).
- [5] J. B. Carter, J. P. Holland, E. Peltzer, B. Richardson, E. Bogle, H. T. Nguyen, Y. Melaku, D. Gates, and M. Ben-Dor, *J. Vac. Sci. Technol. A* **11**, 1301 (1993).
- [6] J. Hopwood, C. R. Guarnieri, S. J. Whitehair, and J. J. Cuomo, *J. Vac. Sci. Technol. A* **11**, 153 (1993).
- [7] L. J. Mahoney, A. E. Wendt, E. Barrios, C. J. Richards, and J. L. Shohet, *J. Appl. Phys.* **76**, 2041 (1994).
- [8] U. Kortshagen, I. Pukropski, and M. Zethoff, *J. Appl. Phys.* **76**, 2048 (1994).
- [9] C. Lai, B. Brunmeier, and R. C. Woods, *J. Vac. Sci. Technol. A* **13**, 2086 (1995).
- [10] P. N. Wainman, M. A. Lieberman, A. J. Lichtenberg, R. A. Stewart, and C. Lee, *J. Vac. Sci. Technol. A* **13**, 2464 (1995).
- [11] J. A. Meyer and A. E. Wendt, *J. Appl. Phys.* **78**, 90 (1995).
- [12] D. F. Beale, A. E. Wendt, and L. J. Mahoney, *J. Vac. Sci. Technol. A* **12**, 2775 (1994).
- [13] J. A. O'Neill, M. S. Barnes, and J. H. Keller, *J. Appl. Phys.* **73**, 1621 (1993).
- [14] T. Hori, M. D. Bowden, K. Uchino, K. Muraoka, and M. Maeda, *J. Vac. Sci. Technol. A* **14**, 144 (1996).
- [15] P. J. Hargis, Jr., K. E. Greenberg, P. A. Miller, J. B. Gerado, J. R. Torczynski, M. E. Riley, G. A. Hebner, J. R. Roberts, J. K. Olthoff, J. R. Whetstone, R. J. Van Brunt, M. A. Sobolewski, H. M. Anderson, M. P. Splichal, J. L. Mock, P. Bletzinger, A. Garscadden, R. A. Gottscho, G. Selwyn, M. Dalvie, J. E. Heidenreich, J. W. Butterbaugh, M. L. Brake, M. L. Passow, J. Pender, A. Lujan, M. E. Elta, D. B. Graves, H. H. Sawin, M. J. Kushner, J. T. Verdeyen, R. Horwath, and T. R. Turner, *Rev. Sci. Instrum.* **65**, 140 (1994).
- [16] P. A. Miller, G. A. Hebner, K. E. Greenberg, P. D. Pochan, and B. P. Aragon, *J. Res. Natl. Inst. Stand. Technol.* **100**, 427 (1995).
- [17] P. A. Chatterton, J. A. Rees, N. L. Wu, and K. Al-Assadi, *Vacuum* **42**, 489 (1991).
- [18] V. A. Godyak, R. B. Piejak, and B. M. Alexandrovich, *Plasma Sources Sci. Technol.* **1**, 36 (1992).
- [19] V. A. Godyak and R. B. Piejak, *J. Appl. Phys.* **68**, 3157 (1990).
- [20] M. A. Sobolewski, *IEEE Trans. Plasma Sci.* **23**, 1006 (1995).
- [21] U. Flender, B. H. Nguyen Thi, and K. Wiesemann, *Plasma Sources Sci. Technol.* **5**, 61 (1996).
- [22] L. Schott, in *Plasma Diagnostics*, edited by W. Lochte-Holtgreven (North-Holland, Amsterdam, 1968).
- [23] M. Petig, *Report No. 92-17-24, SFB Neidertemperaturplasmen* (Arbeitsgemeinschaft Plasmaphysik, Bochum, 1992) (in German).
- [24] M. J. Druyvesteyn, *Z. Phys.* **64**, 781 (1930).
- [25] V. A. Godyak, R. B. Piejak, and B. M. Alexandrovich, *J. Appl. Phys.* **73**, 3657 (1993).
- [26] U. Flender and K. Wiesemann, *Plasma Chem. Plasma Process.* **15**, 123 (1995).
- [27] D. Rapp and D. D. Briglia, *J. Chem. Phys.* **43**, 1480 (1965).
- [28] L. Vejby-Christensen, D. Kella, D. Mathur, H. B. Petersen, H. T. Schmidt, and L. H. Andersen, *Phys. Rev. A* **53**, 2371 (1996).
- [29] F. C. Fehsenfeld, A. L. Schmeltekopf, H. I. Schiff, and E. E. Ferguson, *Planet. Space Sci.* **15**, 373 (1967).
- [30] G. A. Hebner, *J. Appl. Phys.* **80**, 2624 (1996).
- [31] J. B. Thompson, *Proc. R. Soc. London. Ser. A* **262**, 503 (1961).
- [32] H. Amemiya, *J. Phys. Soc. Jpn.* **57**, 887 (1988).
- [33] V. A. Godyak, R. B. Piejak, and B. M. Alexandrovich, *Plasma Sources Sci. Technol.* **4**, 332 (1995).
- [34] V. I. Kolobov, G. J. Parker, and W. N. G. Hitchon, *Phys. Rev. E* **53**, 1110 (1996).
- [35] U. Kortshagen, I. Pukropski, and L. D. Tsendin, *Phys. Rev. E* **51**, 6063 (1995).